Published in final edited form as:
Mol Pharm. 2013 February 4; 10(2): 709–716. doi:10.1021/mp300507r.

Positron Emission Tomography Imaging of Tumor Angiogenesis with a $^{61/64}$Cu-Labeled F(ab')$_2$ Antibody Fragment

Hao Hong[1,#], **Yin Zhang**[2,#], **Hakan Orbay**[1], **Hector F. Valdovinos**[2], **Tapas R. Nayak**[1], **Jero Bean**[1], **Charles P. Theuer**[3], **Todd E. Barnhart**[2], and **Weibo Cai**[1,2,4,*]

[1]Department of Radiology, University of Wisconsin - Madison, WI, USA

[2]Department of Medical Physics, University of Wisconsin - Madison, WI, USA

[3]TRACON Pharmaceuticals, Inc., San Diego, CA, USA

[4]University of Wisconsin Carbone Cancer Center, Madison, WI, USA

Abstract

The objective of this study was to characterize the in vitro and in vivo properties of the F(ab')$_2$ fragment of TRC105, a human/murine chimeric IgG1 monoclonal antibody that binds with high avidity to human and murine CD105 (i.e. endoglin), and investigate its potential for positron emission tomography (PET) imaging of tumor angiogenesis after $^{61/64}$Cu-labeling. TRC105-F(ab')$_2$ of high purity was produced by pepsin digestion of TRC105, which was confirmed by SDS-PAGE, HPLC analysis, and mass spectrometry. $^{61/64}$Cu-labeling of NOTA-TRC105-F(ab')$_2$ (NOTA denotes 1,4,7-triazacyclononane-1,4,7-triacetic acid) was achieved with yields of > 75% (specific activity: ~115 GBq/μmol). PET imaging revealed rapid tumor uptake of ^{64}Cu-NOTA TRC105-F(ab')$_2$ in the 4T1 murine breast cancer model (5.8 ± 0.8, 7.6 ± 0.6, 5.6 ± 0.4, 5.0 ± 0.6, and 3.8 ± 0.7 %ID/g at 0.5, 3, 16, 24, and 48 h post-injection respectively; n = 4). Since tumor uptake peaked at 3 h post-injection, ^{61}Cu-NOTA-TRC105-F(ab')$_2$ also gave good tumor contrast at 3 and 8 h post-injection. CD105 specificity of the tracers was confirmed by blocking studies and histopathology. In conclusion, the use of a F(ab')$_2$ fragment led to more rapid tumor uptake (which peaked at 3 h post-injection) than radiolabeled intact antibody (which often peaked after 24 h post-injection), which may allow for same day immunoPET imaging in future clinical studies.

Keywords

Positron emission tomography (PET); Tumor angiogenesis; Antibody fragment; F(ab')$_2$; CD105 (endoglin); Breast cancer; ^{61}Cu; ^{64}Cu

INTRODUCTION

Malignant tumors depend on angiogenesis to grow and metastasize.[1] During the last decade, molecular imaging of tumor angiogenesis has been an extremely dynamic research area.[2–6] Some of the most intensively studied angiogenesis-related targets are integrin $\alpha_v\beta_3$, vascular endothelial growth factor receptors (VEGFRs), CD105 (i.e. endoglin), among others.[2–5, 7–9] Several tracers targeting these receptors are already undergoing clinical investigation.[3, 4, 9]

[*]**Requests for reprints:** Weibo Cai, PhD, Departments of Radiology and Medical Physics, University of Wisconsin - Madison, Room 7137, 1111 Highland Avenue, Madison, WI 53705-2275, USA wcai@uwhealth.org; Phone: 608-262-1749; Fax: 608- 265-0614.
[#]These authors contributed equally to this work

CONFLICT OF INTEREST C.P.T. is an employee of TRACON Pharmaceuticals, Inc. The other authors declare that they have no conflict of interest.

CD105 is a disulfide-linked homodimeric cell membrane glycoprotein that is primarily overexpressed on proliferating endothelial cells, which makes it a promising vascular target for diagnostic, prognostic, and therapeutic applications.[8, 10, 11]

High CD105 expression correlates with poor prognosis in more than 10 solid tumor types, including breast cancer.[10] CD105 microvessel density (MVD) by immunohistochemistry (IHC) is the accepted approach for assessing tumor neovascularization, a quantitative measure of tumor angiogenesis. To date, positron emission tomography (PET) imaging of CD105 has not been investigated in the clinic. We reported the first PET imaging of CD105 expression in a mouse model of breast cancer, using the chimeric monoclonal antibody TRC105 as the targeting moiety.[12] When compared with other anti-CD105 antibodies, TRC105 has a very high avidity for both human and murine CD105. A multicenter Phase 1 first-in-human dose-escalation trial of TRC105 was recently completed in the United States and multiple Phase 2 therapy trials are underway in patients with various solid tumor types.[13] Translation of the optimized PET tracer(s) into the clinic for CD105 imaging (i.e. non-invasive full body MVD measurement) may play multiple roles in improving the management of cancer patients.

One limitation of PET imaging with radiolabeled intact antibodies is the prolonged circulation half-life,[14] hence tumor uptake typically does not peak until a few days after tracer injection. This has led to the development of antibody fragment-based PET tracers that can exhibit specific targeting (e.g. with bivalent binding to the antigen) and rapid blood clearance to allow for potential same day immunoPET imaging in clinical investigation.[15–18] IgG antibodies are composed of Fc and Fab fragments, with the Fab fragments containing the antigen binding sites. Fab and $F(ab')_2$ fragments can be produced from monoclonal antibodies by enzymatic digestion using papain and pepsin, respectively.[19, 20] These Fab and $F(ab')_2$ fragments maintain the same antigenic specify as the parent antibody, while possessing the potential advantages of better solid tumor penetration and faster clearance because of their smaller sizes (~50 kDa and ~100 kDa respectively) than the parent antibody (~150 kDa).

We hypothesized that radiolabeled $F(ab')_2$ fragments, by maintaining bivalency with substantially reduced size, would exhibit better performance for in vivo imaging applications than the parent antibody. The goal of this study was to investigate the in vitro and in vivo characteristics of ^{64}Cu-labeled TRC105-$F(ab')_2$ for PET imaging of tumor angiogenesis in a 4T1 murine breast cancer model. Since radiolabeled $F(ab')_2$ is expected to have rapid blood clearance and tumor uptake, ^{61}Cu-labeling may also provide sufficient tumor contrast at early time points. ^{61}Cu, which has a higher β^+ branching ratio (60% vs. 17%) and shorter decay half-life (3.4 h vs. 12.7 h) than ^{64}Cu, can provide stronger PET signal and lower radiation dosimetry to normal organs.

EXPERIMENTAL SECTION

Chemicals

TRC105 was provided by TRACON pharmaceuticals Inc. (San Diego, CA). AlexaFluor488- and Cy3-labeled secondary antibodies were purchased from Jackson Immunoresearch Laboratories, Inc. (West Grove, CA). *p*-SCN-Bn-NOTA (i.e. 2-S-(4-isothiocyanatobenzyl)-1,4,7-triazacyclononane-1,4,7-triacetic acid) was acquired from Macrocyclics, Inc. (Dallas, TX). Pepsin, fluorescein isothiocyanate (FITC), hematoxylin staining solution, and Chelex 100 resin (50–100 mesh) were purchased from Sigma-Aldrich (St. Louis, MO). AlexaFluor350-NHS (NHS denotes N-hydroxysuccinimide) ester was acquired from Invitrogen (Grand island, NY). Water and all buffers were of Millipore grade and pre-treated with Chelex 100 resin to ensure that the aqueous solution was heavy metal-

free. PD-10 columns were purchased from GE Healthcare (Piscataway, NJ). Dionex ProPac WCX-10 weak cation-exchange column (4 × 250 mm) and all other reaction buffers and chemicals were purchased from Thermo Fisher Scientific (Fair Lawn, NJ).

Generation and Characterization of TRC105-F(ab')$_2$

The pH of TRC105 solution (2 mg/mL) was adjusted with 0.1 N HCl to ~3.5. Pepsin was dissolved in sodium acetate buffer (2 mg/mL) and added to the TRC105 solution, with pepsin:TRC105 weight ratios of 1:500, 1:100, 1:50, 1:25, or 1:10. The mixtures were incubated at 37 °C and the time of digestion was varied from 1 to 24 h, which was terminated by adjusting the pH value of the mixtures to 8 using a 0.1 N NaOH solution. After identifying the optimal digestion condition, TRC105-F(ab')$_2$ was purified by Sephadex G-75 size exclusion column chromatography with phosphate-buffered saline (PBS) as the mobile phase. The concentration of TRC105-F(ab')$_2$ was determined based on UV absorbance at 280 nm, using an extinction coefficient of 1.45 mL/mg/cm.[21]

The purity of TRC105-F(ab')$_2$ was evaluated with sodium dodecyl sulfate polyacrylamide gel electrophoresis (SDS-PAGE, 5% stacking gel and 8% resolving gel) under non-reducing conditions using Coomassie brilliant blue R-250 staining. The molecular weight of TRC105-F(ab')$_2$ was determined by matrix-assisted laser desorption/ionization (MALDI) mass spectrometry, which served as a reference for determining the location of the TRC105-F(ab')$_2$ band in SDS-PAGE.

In addition, high performance liquid chromatography (HPLC) analysis was conducted for both TRC105-F(ab')$_2$ and TRC105 in a Dionex Ultimate 3000 HPLC system using the ProPac WCX-10 column. Eluent A: 20 mM 2-(*N*-morpholino)ethanesulfonic acid (MES), 1 mM ethylenediaminetetraacetic acid (EDTA), 20 mM NaCl, pH 5.5; Eluent B: 20 mM MES, 1 mM EDTA, 250 mM NaCl, pH 5.5. The NaCl gradient used was 3.75 mM/min with a flow rate of 1 mL/min. Absorbance at 280 nm was used for protein detection.

NOTA/FITC/AlexaFluor350 Conjugation and $^{61/64}$Cu-Labeling of TRC105-F(ab')$_2$

NOTA conjugation was carried out at pH 9.0, with the reaction ratio of *p*-SCN-Bn-NOTA:TRC105-F(ab')$_2$ being 20:1. NOTA-F(ab')$_2$ was purified using PD-10 columns with PBS as the mobile phase. Similar reaction condition was adopted for conjugation of FITC or AlexaFluor350-NHS ester onto TRC105-F(ab')$_2$, except the ratio of FITC or AlexaFluor350-NHS ester:TRC105-F(ab')$_2$ was 3:1 to avoid self-quenching of the fluorescence signal.

The two copper isotopes were produced with an on-site cyclotron (GE PETtrace) using ^{60}Ni(d,n)^{61}Cu and ^{64}Ni(p,n)^{64}Cu reactions, respectively. 61Cu has a specific activity of ~2 Ci/μmol and ^{64}Cu has a specific activity of ~5 Ci/μmol at the end of bombardment. ^{61}CuCl$_2$ or ^{64}CuCl$_2$ (74 MBq) was diluted in 300 μL of 0.1 M sodium acetate buffer (pH 6.5) and added to 50 μg of TRC105-F(ab')$_2$. The reaction mixture was incubated for 30 min at 37 °C with constant shaking. $^{61/64}$Cu-NOTA-TRC105-F(ab')$_2$ was purified using PD-10 columns with PBS as the mobile phase. The radioactive fractions containing $^{61/64}$Cu-NOTA-TRC105-F(ab')$_2$ were collected and passed through a 0.2 μm syringe filter before in vivo experiments.

Flow Cytometry

The binding affinity of TRC105-F(ab')$_2$ for CD105 was evaluated with fluorescence-activated cell sorting (FACS) analysis in two cell lines: human umbilical vein endothelial cells (HUVECs, high CD105 expression[12, 22]) and MCF-7 human breast cancer cells (CD105-negative[12, 23]). Briefly, cells were harvested and suspended in cold PBS (pH 7.4)

with 2% bovine serum albumin at a concentration of 5×10^6 cells/mL. The cells were incubated with various concentrations of FITC-TRC105-F(ab')$_2$ (5, 25, or 100 nM) for 30 min at room temperature, washed three times with cold PBS, and centrifuged at 1,000 rpm for 5 min. Afterwards, the cells were washed and analyzed by FACS using a BD FACSCalibur 4-color analysis cytometer, which is equipped with 488 nm and 633 nm lasers (Becton-Dickinson, San Jose, CA) and FlowJo analysis software (Tree Star, Inc., Ashland, OR).

PET Imaging and Biodistribution Studies

The 4T1 murine breast cancer model was generated as previously described.[12, 24] PET scans of 4T1 tumor-bearing mice were performed using an Inveon microPET/microCT rodent model scanner (Siemens Medical Solutions USA, Inc.). Each mouse was intravenously injected with 5–10 MBq of $^{61/64}$Cu-NOTA-TRC105-F(ab')$_2$ and 5 or 10 minute static PET scans were performed at various time points post-injection (p.i.). The images were reconstructed using a maximum a posteriori (MAP) algorithm, with no attenuation or scatter correction. Region-of-interest (ROI) analysis of each PET scan was performed using vendor software (Inveon Research Workplace [IRW]) on decay-corrected whole-body images as described previously,[25, 26] to calculate the percentage injected dose per gram of tissue (%ID/g) values for the 4T1 tumor and several major organs.

Blocking studies were carried out to evaluate CD105 specificity of ^{64}Cu-NOTA-TRC105-F(ab')$_2$ in vivo, where a group of 4 mice was each injected with 1 mg of TRC105 within 1 h before ^{64}Cu-NOTA-TRC105-F(ab')$_2$ administration. A subset of mice was also subjected to CT scans, with a voxel resolution of 210 μm. Fiducial markers were used for co-registration, and images were reconstructed using the vendor software (Inveon Acquisition Workplace; Siemens). The CT and PET data sets were registered via rigid registration in IRW.

At 3 and 48 h p.i., cohorts of mice were euthanized and the blood, 4T1 tumor, and major organs/tissues were collected and wet-weighed. The radioactivity in the tissue was measured using a Packard Cobra II gamma-counter (Perkin-Elmer; energy window: 400 – 600 keV) and presented as %ID/g. The 4T1 tumor, liver, kidney (i.e., tissues with significant uptake of $^{61/64}$Cu-NOTA-TRC105-F(ab')$_2$), and muscle were also frozen and sectioned for histological analysis after the decay of radioactivity.

Histology

Frozen tissue slices of 7 μm thickness were fixed with cold acetone for 10 min and dried in the air for 30 min. After rinsing with PBS and blocking with 10% donkey serum for 30 min at room temperature, the slices were incubated with TRC105 (2 μg/mL) for 1 h at 4 °C and visualized using AlexaFluor488-labeled goat anti-human IgG. After washing with PBS, the tissue slices were also stained for endothelial marker CD31 as described previously.[12] Subsequently, the slices were incubated with AlexaFluor350-TRC105-F(ab')$_2$ (2 μg/mL) for 30 min. Hematoxylin staining was also carried out to demarcate the cell nuclei in the tissue slices. After final wash with PBS, all images were acquired with a Nikon Eclipse Ti microscope.

Statistical Analysis

Quantitative data were expressed as mean ± SD. Means were compared using Student's *t* test. P values < 0.05 were considered statistically significant.

RESULTS

Optimization of TRC105-F(ab')$_2$ Generation and Purification

Pilot studies of digestion time at 37 °C at a fixed pepsin:TRC105 ratio of 1:50 revealed that a digestion time of 4 h was optimal for generating TRC105-F(ab')$_2$ without significant presence of intact TRC105. Therefore, a digestion period of 4 h was adopted for all subsequent experiments. The effect of pepsin:TRC105 ratio on the digestion process at 37 °C for a 4 h period was investigated by varying the pepsin:TRC105 ratio from 1:500 to 1:10 (w/w). A pepsin:TRC105 ratio of 1:100 was found to completely digest TRC105 to its F(ab')$_2$ fragment, and further increase in pepsin concentration did not lead to significant benefit. Therefore, the pepsin:TRC105 ratio of 1:100 was used to generate TRC105-F(ab')$_2$ for further in vitro and in vivo studies.

Sephadex G-75 (fractionation molecular weight range: 3,000 – 70,000 Da) was used to purify TRC105-F(ab')$_2$ from the reaction mixture (which contains TRC105-Fc, pepsin, TRC105-Fab, etc.). A sample elution profile is shown in Figure 1A and only the fraction with the highest TRC105-F(ab')$_2$ concentration was used for further studies (indicated by arrowhead). Following pepsin digestion, SDS-PAGE indicated the disappearance of the band corresponding to TRC105 and the appearance of TRC105-F(ab')$_2$, TRC105-Fc, and several other lower molecular weight species (Figure 1B). The purity of TRC105-F(ab')$_2$ following Sephadex G-75 purification was confirmed by SDS-PAGE (lane 4 in Figure 1B) and HPLC (Figure 1C). Taken together, these findings indicated complete TRC105 digestion by pepsin treatment to yield pure TRC105-F(ab')$_2$ for further conjugation and investigation. Mass spectrometry indicated that the molecular mass of TRC105 and TRC105-F(ab')$_2$ were ~148 kDa and ~97 kDa, respectively (Figure 1D).

Flow Cytometry Analysis

Treatment of HUVECs with FITC-TRC105-F(ab')$_2$ at 25 nM enhanced the mean fluorescence intensity by ~20 fold compared to the unstained cells, whereas treatment with a “blocking” dose of TRC105 (1 μM) reduced the cell fluorescence by ~10 fold (Figure 2). Fluorescence signal on CD105 negative MCF-7 cells was minimal for all groups even when treated with FITC-TRC105-F(ab')$_2$ at a much higher concentration of 100 nM, indicating low non-specific binding of FITC-TRC105-F(ab')$_2$ in cell culture. Together, FACS studies revealed that FITC-TRC105-F(ab')$_2$ exhibited specific binding to CD105 on cells with minimal non-specific binding, indicating that pepsin digestion did not compromise the CD105 binding avidity of TRC105-F(ab')$_2$ and warranted further in vivo investigation of $^{61/64}$Cu-labeled TRC105-F(ab')$_2$.

In Vivo PET Imaging and Biodistribution Studies

$^{61/64}$Cu-labeling, including purification using PD-10 columns, took 60 ± 10 min (n = 8). The decay-corrected radiochemical yield was 77.6 ± 7.1%, based on 25 μg of NOTA-TRC105-F(ab')$_2$ per 37 MBq of $^{61/64}$Cu, with radiochemical purity of >95%. The specific activity was ~115 GBq/μmol for $^{61/64}$Cu-NOTA-TRC105-F(ab')$_2$, assuming complete recovery of NOTA-TRC105-F(ab')$_2$ after size exclusion chromatography.

Coronal PET images that contain the 4T1 tumors are shown in Figure 3A and a representative PET/CT fused image of a mouse at 3 h p.i. of ^{64}Cu-NOTA-TRC105-F(ab')$_2$ is shown in Figure 3B. ^{61}Cu-NOTA-TRC105-F(ab')$_2$ exhibited a similar in vivo distribution pattern as ^{64}Cu-NOTA-TRC105-F(ab')$_2$ at early time points (Figure 3C). Quantitative data obtained from ROI analysis of the PET results are shown in Figure 4.

Due to the smaller size compared to the parent antibody TRC105, ^{64}Cu-NOTA-TRC105-F(ab')$_2$ was cleared through both the hepatobiliary and renal pathways. The liver take of ^{64}Cu-NOTA-TRC105-F(ab')$_2$ was 22.4 ± 2.9, 19.7 ± 2.0, 14.6 ± 1.9, 13.8 ± 1.3, and 10.0 ± 0.8 %ID/g at 0.5, 3, 16, 24, and 48 h p.i respectively (n = 4; Figure 4A). Radioactivity in the blood was 10.7 ± 1.8, 4.9 ± 1.1, 3.1 ± 0.6, 2.7 ± 1.3, and 2.4 ± 0.6 %ID/g at 0.5, 3, 16, 24, and 48 h p.i respectively (n = 4; Figure 4A), indicating faster clearance from the blood than ^{64}Cu-NOTA-TRC105 (which had blood radioactivity level of 16.2 ± 1.9, 10.7 ± 2.0, and 8.3 ± 0.9 %ID/g at 4, 24, and 48 h p.i. respectively; n = 3).[27] Importantly, tumor uptake of ^{64}Cu-NOTA-TRC105-F(ab')$_2$ accumulated rapidly and was clearly visible at 0.5 h p.i., peaked at 3 h p.i., and remained prominent over time (5.8 ± 0.8, 7.6 ± 0.6, 5.6 ± 0.4, 5.0 ± 0.6, and 3.8 ± 0.7 %ID/g at 0.5, 3, 16, 24, and 48 h p.i respectively; n = 4; Figure 4A). As a comparison, uptake of ^{64}Cu-NOTA-TRC105 in the 4T1 tumor was visible at 4 h p.i. and plateaued after 24 h p.i. (7.5 ± 2.7, 11.4 ± 1.9, and 13.0 ± 1.2 %ID/g at 4, 24, and 48 h p.i. respectively; n = 3).[27] Because of the rapid clearance and tumor uptake of radiolabeled TRC105-F(ab')$_2$, ^{61}Cu-labeling was also sufficient to provide good tumor contrast at the time points of 3 and 8 h p.i. (Figure 3C).

Administering a blocking dose of TRC105 1 h prior to ^{64}Cu-NOTA-TRC105-F(ab')$_2$ injection significantly reduced tumor uptake to 2.1 ± 0.4, 2.6 ± 0.3, 2.5 ± 0.4, 2.5 ± 0.4, and 2.4 ± 0.7 %ID/g at 0.5, 3, 16, 24, and 48 h p.i respectively (n = 4; $P < 0.05$ before 48 h p.i.; Figure 3A, 4B&C), which demonstrated that ^{64}Cu-NOTA-TRC105-F(ab')$_2$ maintained the CD105 specificity of its parent antibody in vivo. Liver uptake of ^{64}Cu-NOTA-TRC105-F(ab')$_2$ in the "blocking" group was similar to mice injected with ^{64}Cu-NOTA-TRC105-F(ab')$_2$ alone, at 18.0 ± 2.5, 16.3 ± 1.6, 11.1 ± 1.7, 10.0 ± 2.0, and 8.0 ± 1.4 %ID/g at 0.5, 3, 16, 24, and 48 h p.i respectively (n = 4). Radioactivity in the blood (10.3 ± 2.7, 4.4 ± 2.0, 2.9 ± 0.2, 2.8 ± 0.2, and 2.4 ± 0.4 %ID/g at 0.5, 3, 16, 24, and 48 h p.i respectively; n = 4) was also similar between the two groups (Figure 4A&B).

Following the last PET scans at 48 h p.i., biodistribution studies confirmed that quantitative tracer uptake values based on PET imaging accurately reflected radioactivity distribution in tumor-bearing mice, as similar %ID/g values were obtained from PET and biodistribution studies (Figure 5B). In addition, 2 other groups of four 4T1 tumor-bearing mice were intravenously injected with ^{64}Cu-NOTA-TRC105-F(ab')$_2$, or ^{64}Cu-NOTA-TRC105-F(ab')$_2$ with a pre-injected blocking dose of TRC105, and euthanized at 3 h p.i. (when tumor uptake was at the peak based on PET results) for biodistribution studies. Both the liver and kidneys (i.e. the clearance organs for the tracer) had significant tracer uptake at 3 h p.i. for ^{64}Cu-NOTA-TRC105-F(ab')$_2$ (Figure 5A). More importantly, the 4T1 tumor uptake of ^{64}Cu-NOTA-TRC105-F(ab')$_2$ was higher than all major organs except the liver, thus providing good tumor contrast.

The peak uptake in the 4T1 tumor was lower for ^{64}Cu-NOTA-TRC105-F(ab')$_2$ (7.6 ± 0.6 %ID/g at 3 h p.i; n = 4) than ^{64}Cu-NOTA-TRC105 (13.0 ± 1.2 %ID/g at 48 h p.i.; n = 3), which is expected for radiolabeled antibody fragments.[28] However, the tumor-to-blood ratios were significantly better at early time points for ^{64}Cu-NOTA-TRC105-F(ab')$_2$ (1.6 ± 0.2, 1.8 ± 0.3, and 1.6 ± 0.3 for 3, 24, 48 h p.i. respectively; n = 4) than ^{64}Cu-NOTA-TRC105 (0.5 ± 0.1, 1.0 ± 0.2, and 1.6 ± 0.2 for 4, 24, and 48 h p.i. respectively; n = 3), which is desirable for future clinical translation where same day PET imaging after tracer injection can be achieved. In addition, the possible use of shorter-lived ^{61}Cu instead of ^{64}Cu as the radiolabel can not only increase the PET signal intensity (due to a higher β^+ branching ratio) but also reduce the radiation dosimetry to normal organs (due to a shorter decay half-life).

Histology

Immunofluorescence CD105/CD31 co-staining of various tissues revealed that CD105 expression in the 4T1 tumor was primarily on the tumor vasculature, as evidenced by excellent co-localization of CD105 and CD31 staining and very weak signal on the 4T1 tumor cells (Figure 6). CD105 staining of mouse liver and kidney both gave very low signal, indicating that these tissues do not have significant CD105 expression. Thus, uptake of $^{61/64}$Cu-NOTA-TRC105-F(ab')$_2$ in the liver/kidneys was largely attributed to hepatic/renal clearance instead of CD105 binding. The staining with AlexaFluor350-TRC105-F(ab')$_2$ provided excellent overlay with both CD105 and CD31 staining in the 4T1 tumor, which suggested that TRC105-F(ab')$_2$ and $^{61/64}$Cu-NOTA-TRC105-F(ab')$_2$ bind specifically to CD105 on the tumor vasculature.

DISCUSSION

CD105 has emerged as a unique marker of proliferating (activated) endothelial cells in vitro and in vivo.[11, 13, 29] Although the exact roles of CD105 in endothelial cell signaling is complex and remains to be completely elucidated, its potential as a target for imaging and therapy of solid tumors has been well established. We have previously shown that radiolabeled TRC105 can be used for in vivo PET imaging of CD105 expression.[12, 22] In comparison to other targets for tumor imaging, CD105 exhibits several potential advantages such as lack of tumor histotype specificity, independence from its expression on neoplastic cells, immediate accessibility of malignant lesions through the blood stream, and overexpression in a wide variety of solid malignancies because of tumor-associated neovascularization. The efficacy of the murine parent antibody of TRC105 (i.e. SN6j) has been demonstrated in many preclinical studies,[29] and several Phase 2 studies using TRC105 (as a single agent or in combination with other drugs) are ongoing after promising findings from the Phase 1 study.[13] Development and clinical translation of a PET tracer for imaging of CD105 expression in cancer patients may significantly facilitate future clinical trials through more accurate patient selection for enrollment, as well as monitoring the efficacy of therapies targeting CD105 and other angiogenesis-related targets.

The major limitations of antibody-based molecular imaging are slow uptake of the labeled antibody in the tumor tissue (due to the long circulation half-lives of most antibodies) and high background signal in the blood and the reticuloendothelial system (i.e. liver).[14] Therefore, many literature reports have involved the use of F(ab')$_2$ antibody fragments for imaging applications to achieve faster tumor penetration and blood clearance.[15, 30, 31] In this study, ^{64}Cu-NOTA-TRC105-F(ab')$_2$ had much faster blood clearance than similarly labeled TRC105, which enabled the use of shorter lived PET isotope (i.e. ^{61}Cu) since tumor uptake of ^{64}Cu-NOTA-TRC105-F(ab')$_2$ peaked at around 3 h p.i. A similar tumor uptake pattern was observed for ^{61}Cu-NOTA-TRC105-F(ab')$_2$ as the ^{64}Cu-labled tracer. While ^{64}Cu can have both diagnostic and therapeutic applications, ^{61}Cu is mainly a diagnostic isotope. It has been shown that the tomographic images obtained using ^{61}Cu are superior to those using ^{64}Cu, due to higher β^+ branching ratio.[32] In addition, the use of ^{61}Cu decreases the radiation dose to the normal tissues, and the production of ^{61}Cu is less costly than ^{64}Cu with the use of a deuteron beam for ^{61}Cu production (^{60}Ni is significantly less expensive than ^{64}Ni). For imaging/diagnostic purposes using radiolabeled antibody F(ab')$_2$/Fab fragments, ^{61}Cu may serve as a preferred isotope compared to the more widely available ^{64}Cu. Several other PET isotopes also have desirable characteristics for antibody fragment-based imaging (e.g. ^{45}Ti and ^{44}Sc have similar half-life to ^{61}Cu and higher β^+ branching ratio), which deserve investigation in the near future.

Interestingly, a slight decline in tumor uptake of ^{64}Cu-NOTA-TRC105-F(ab')$_2$ was observed after 16 h p.i. We propose that this phenomenon may be due to the lower internalization

efficiency of ^{64}Cu-NOTA-TRC105-F(ab')$_2$ compared to ^{64}Cu-NOTA-TRC105 after CD105 binding, because of the lack of Fc which can play a significant role in antibody internalization. ^{64}Cu can be efficiently trapped once internalized into cells, which can lead to accumulation of tumor uptake over time, while ^{64}Cu outside the cells can be readily cleared once the tracer is metabolized. One advantage of F(ab')$_2$ fragment is that it can eliminate non-specific binding between the Fc portion of antibodies and Fc receptors on various types of cells (e.g. macrophages, dendritic cells, neutrophils, natural killer cells, B cells etc.).[33] The lower uptake of ^{64}Cu-NOTA-TRC105-F(ab')$_2$ in the mouse spleen (3.9 ± 0.3 and 2.6 ± 0.1 %ID/g at 3 h and 48 h p.i.; n = 4) than ^{64}Cu-NOTA-TRC105 (4.8 ± 0.2 and 5.2 ± 0.5 %ID/g at 24 h and 48 h p.i.; n = 3) may reflect this aspect. Furthermore, the use of radiolabeled F(ab')$_2$ for imaging may be more suitable than labeled intact antibodies as the latter may be more likely to generate immune responses.

The rationale for choosing the 4T1 tumor model for this study is that the parent antibody (i.e. SN6j) of TRC105 has been shown to be effective as an anti-angiogenic agent in this model.[34] Further, this is a rapidly growing tumor model that contains highly angiogenic tumor vasculature which can provide sufficient target density for imaging applications. Since there are significantly fewer tumor vascular endothelial cells than tumor cells, which are the targets of most antibodies used for cancer imaging, tumor uptake of TRC105-based PET tracers is often lower than other antibody (fragment)-based tracers.[25, 35–37] One limitation of this model is that the tumor vasculature is of murine origin. TRC105 has significantly higher affinity to human CD105 than its murine homolog.[38] Therefore, it is possible that the tracer will perform better in cancer patients than what was observed in this study. Lastly, the use of radiolabeled Fab fragment can also be investigated for PET studies, which may also give good tumor contrast despite the monovalent structure.

CONCLUSION

Herein we report the development, characterization, and in vivo investigation of $^{61/64}$Cu-labeled F(ab')$_2$ fragment of TRC105 in a mouse model of breast cancer. Both ^{61}Cu- and ^{64}Cu-labeled TRC105-F(ab')$_2$ exhibited rapid, prominent, and target-specific uptake in the 4T1 tumor. The use of a F(ab')$_2$ fragment led to much faster tumor uptake than the similarly labeled intact antibody, which may be translated into same day immunoPET imaging in the clinic.

Acknowledgments

This work is supported, in part, by the University of Wisconsin Carbone Cancer Center, the Department of Defense (W81XWH-11-1-0644), and the Elsa U. Pardee Foundation.

REFERENCES

(1). Carmeliet P, Jain RK. Angiogenesis in cancer and other diseases. Nature. 2000; 407:249–57. [PubMed: 11001068]

(2). Cai W, Chen X. Multimodality molecular imaging of tumor angiogenesis. J. Nucl. Med. 2008; 49(Suppl 2):113S–28S. [PubMed: 18523069]

(3). Cai W, Niu G, Chen X. Imaging of integrins as biomarkers for tumor angiogenesis. Curr. Pharm. Des. 2008; 14:2943–73. [PubMed: 18991712]

(4). Dijkgraaf I, Boerman OC. Radionuclide imaging of tumor angiogenesis. Cancer Biother. Radiopharm. 2009; 24:637–47. [PubMed: 20025543]

(5). Cai W, Rao J, Gambhir SS, Chen X. How molecular imaging is speeding up anti-angiogenic drug development. Mol. Cancer Ther. 2006; 5:2624–2633. [PubMed: 17121909]

(6). Wang RE, Niu Y, Wu H, Amin MN, Cai J. Development of NGR peptide-based agents for tumor imaging. Am. J. Nucl. Med. Mol. Imaging. 2011; 1:36–46. [PubMed: 23133793]

(7). Backer MV, Levashova Z, Patel V, Jehning BT, Claffey K, Blankenberg FG, Backer JM. Molecular imaging of VEGF receptors in angiogenic vasculature with single-chain VEGF-based probes. Nat. Med. 2007; 13:504–9. [PubMed: 17351626]

(8). Zhang Y, Yang Y, Hong H, Cai W. Multimodality molecular imaging of CD105 (Endoglin) expression. Int. J. Clin. Exp. Med. 2011; 4:32–42. [PubMed: 21394284]

(9). Cai W, Chen X. Multimodality imaging of vascular endothelial growth factor and vascular endothelial growth factor receptor expression. Front. Biosci. 2007; 12:4267–79. [PubMed: 17485373]

(10). Dallas NA, Samuel S, Xia L, Fan F, Gray MJ, Lim SJ, Ellis LM. Endoglin (CD105): a marker of tumor vasculature and potential target for therapy. Clin. Cancer Res. 2008; 14:1931–7. [PubMed: 18381930]

(11). Fonsatti E, Nicolay HJ, Altomonte M, Covre A, Maio M. Targeting cancer vasculature via endoglin/CD105: a novel antibody-based diagnostic and therapeutic strategy in solid tumours. Cardiovasc. Res. 2010; 86:12–9. [PubMed: 19812043]

(12). Hong H, Yang Y, Zhang Y, Engle JW, Barnhart TE, Nickles RJ, Leigh BR, Cai W. Positron emission tomography imaging of CD105 expression during tumor angiogenesis. Eur. J. Nucl. Med. Mol. Imaging. 2011; 38:1335–43. [PubMed: 21373764]

(13). Rosen LS, Hurwitz HI, Wong MK, Goldman J, Mendelson DS, Figg WD, Spencer S, Adams BJ, Alvarez D, Seon BK, Theuer CP, Leigh B, Gordon MS. A Phase 1 First-in-Human Study of TRC105 (Anti-Endoglin Antibody) in Patients with Advanced Cancer. Clin. Cancer Res. 2012; 18:4820–9. [PubMed: 22767667]

(14). Wu AM, Olafsen T. Antibodies for molecular imaging of cancer. Cancer J. 2008; 14:191–7. [PubMed: 18536559]

(15). Hoeben BA, Kaanders JH, Franssen GM, Troost EG, Rijken PF, Oosterwijk E, van Dongen GA, Oyen WJ, Boerman OC, Bussink J. PET of hypoxia with ^{89}Zr-labeled cG250-F(ab')$_2$ in head and neck tumors. J. Nucl. Med. 2010; 51:1076–83. [PubMed: 20554724]

(16). Leyton JV, Olafsen T, Lepin EJ, Hahm S, Bauer KB, Reiter RE, Wu AM. Humanized radioiodinated minibody for imaging of prostate stem cell antigen-expressing tumors. Clin. Cancer Res. 2008; 14:7488–96. [PubMed: 19010866]

(17). Cai W, Olafsen T, Zhang X, Cao Q, Gambhir SS, Williams LE, Wu AM, Chen X. PET imaging of colorectal cancer in xenograft-bearing mice by use of an ^{18}F-labeled T84.66 anti-carcinoembryonic antigen diabody. J. Nucl. Med. 2007; 48:304–10. [PubMed: 17268029]

(18). Olafsen T, Sirk SJ, Olma S, Shen CK, Wu AM. ImmunoPET using engineered antibody fragments: fluorine-18 labeled diabodies for same-day imaging. Tumour Biol. 2012; 33:669–77. [PubMed: 22392499]

(19). Zhao Y, Gutshall L, Jiang H, Baker A, Beil E, Obmolova G, Carton J, Taudte S, Amegadzie B. Two routes for production and purification of Fab fragments in biopharmaceutical discovery research: Papain digestion of mAb and transient expression in mammalian cells. Protein Expr. Purif. 2009; 67:182–9. [PubMed: 19442740]

(20). Andrew SM, Titus JA. Fragmentation of immunoglobulin G. Curr. Protoc. Immunol. 2001; Chapter 2(Unit 2):8. [PubMed: 18432772]

(21). Kittipongwarakarn S, Hawe A, Tantipolphan R, Limsuwun K, Khomvilai S, Puttipipatkhachorn S, Jiskoot W. New method to produce equine antirabies immunoglobulin F(ab')$_2$ fragments from crude plasma in high quality and yield. Eur. J. Pharm. Biopharm. 2011; 78:189–95. [PubMed: 21414404]

(22). Hong H, Severin GW, Yang Y, Engle JW, Zhang Y, Barnhart TE, Liu G, Leigh BR, Nickles RJ, Cai W. Positron emission tomography imaging of CD105 expression with ^{89}Zr-Df-TRC105. Eur. J. Nucl. Med. Mol. Imaging. 2012; 39:138–48. [PubMed: 21909753]

(23). Fonsatti E, Jekunen AP, Kairemo KJ, Coral S, Snellman M, Nicotra MR, Natali PG, Altomonte M, Maio M. Endoglin is a suitable target for efficient imaging of solid tumors: in vivo evidence in a canine mammary carcinoma model. Clin. Cancer Res. 2000; 6:2037–43. [PubMed: 10815930]

(24). Zhang Y, Hong H, Engle JW, Yang Y, Theuer CP, Barnhart TE, Cai W. Positron emission tomography and optical imaging of tumor CD105 expression with a dual-labeled monoclonal antibody. Mol. Pharm. 2012; 9:645–53. [PubMed: 22292418]

(25). Zhang Y, Hong H, Engle JW, Yang Y, Barnhart TE, Cai W. Positron emission tomography and near-infrared fluorescence imaging of vascular endothelial growth factor with dual-labeled bevacizumab. Am. J. Nucl. Med. Mol. Imaging. 2012; 2:1–13. [PubMed: 22229128]

(26). Zhang Y, Hong H, Severin GW, Engle JW, Yang Y, Goel S, Nathanson AJ, Liu G, Nickles RJ, Leigh BR, Barnhart TE, Cai W. ImmunoPET and near-infrared fluorescence imaging of CD105 expression using a monoclonal antibody dual-labeled with ^{89}Zr and IRDye 800CW. Am. J. Transl. Res. 2012; 4:333–346. [PubMed: 22937210]

(27). Zhang Y, Hong H, Engle JW, Bean J, Yang Y, Leigh BR, Barnhart TE, Cai W. Positron emission tomography imaging of CD105 expression with a ^{64}Cu-labeled monoclonal antibody: NOTA is superior to DOTA. PLoS One. 2011; 6:e28005. [PubMed: 22174762]

(28). Wu AM, Senter PD. Arming antibodies: prospects and challenges for immunoconjugates. Nat. Biotechnol. 2005; 23:1137–46. [PubMed: 16151407]

(29). Seon BK, Haba A, Matsuno F, Takahashi N, Tsujie M, She X, Harada N, Uneda S, Tsujie T, Toi H, Tsai H, Haruta Y. Endoglin-targeted cancer therapy. Curr. Drug Deliv. 2011; 8:135–43. [PubMed: 21034418]

(30). Sandstrom K, Haylock AK, Spiegelberg D, Qvarnstrom F, Wester K, Nestor M. A novel CD44v6 targeting antibody fragment with improved tumor-to-blood ratio. Int. J. Oncol. 2012; 40:1525–32. [PubMed: 22307465]

(31). Zhao D, Stafford JH, Zhou H, Thorpe PE. Near-infrared Optical Imaging of Exposed Phosphatidylserine in a Mouse Glioma Model. Transl. Oncol. 2011; 4:355–64. [PubMed: 22191000]

(32). Williams HA, Robinson S, Julyan P, Zweit J, Hastings D. A comparison of PET imaging characteristics of various copper radioisotopes. Eur. J. Nucl. Med. Mol. Imaging. 2005; 32:1473–80. [PubMed: 16258764]

(33). Ravetch JV, Bolland S. IgG Fc receptors. Annu. Rev. Immunol. 2001; 19:275–90. [PubMed: 11244038]

(34). Tsujie M, Uneda S, Tsai H, Seon BK. Effective anti-angiogenic therapy of established tumors in mice by naked anti-human endoglin (CD105) antibody: differences in growth rate and therapeutic response between tumors growing at different sites. Int. J. Oncol. 2006; 29:1087–94. [PubMed: 17016638]

(35). Dijkers EC, Kosterink JG, Rademaker AP, Perk LR, van Dongen GA, Bart J, de Jong JR, de Vries EG, Lub-de Hooge MN. Development and characterization of clinical-grade ^{89}Zr-trastuzumab for HER2/neu immunoPET imaging. J. Nucl. Med. 2009; 50:974–81. [PubMed: 19443585]

(36). Cai W, Ebrahimnejad A, Chen K, Cao Q, Li ZB, Tice DA, Chen X. Quantitative radioimmunoPET imaging of EphA2 in tumor-bearing mice. Eur. J. Nucl. Med. Mol. Imaging. 2007; 34:2024–36. [PubMed: 17673999]

(37). Cai W, Wu Y, Chen K, Cao Q, Tice DA, Chen X. *In vitro* and *in vivo* characterization of ^{64}Cu-labeled Abegrin™, a humanized monoclonal antibody against integrin $\alpha_v\beta_3$. Cancer Res. 2006; 66:9673–81. [PubMed: 17018625]

(38). Matsuno F, Haruta Y, Kondo M, Tsai H, Barcos M, Seon BK. Induction of lasting complete regression of preformed distinct solid tumors by targeting the tumor vasculature using two new anti-endoglin monoclonal antibodies. Clin. Cancer Res. 1999; 5:371–82. [PubMed: 10037187]

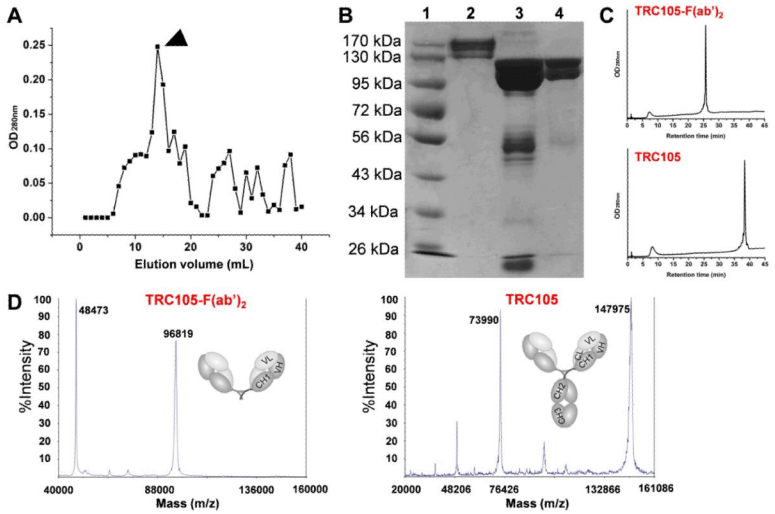

Figure 1.

Production, purification, and characterization of TRC105-F(ab')$_2$. (A) Purification of TRC105-F(ab')$_2$ using a Sephadex G-75 column. Arrowhead indicates the fraction used for further in vitro/in vivo studies. (B) SDS-PAGE to confirm the purity of TRC105-F(ab')$_2$ after Sephadex G-75 column purification. Lane 1: molecular weight markers; lane 2: TRC105; lane 3: reaction mixture after pepsin digestion; lane 4: Purified TRC105-F(ab')$_2$. (C) HPLC analysis further confirmed the purity of TRC105-F(ab')$_2$. (D) Mass spectrometry of TRC105-F(ab')$_2$ (~97 kDa) and its parent antibody TRC105 (~148 kDa). Doubly charged ions are also observed (48,473 Da and 73,990 Da) in the mass spectra.

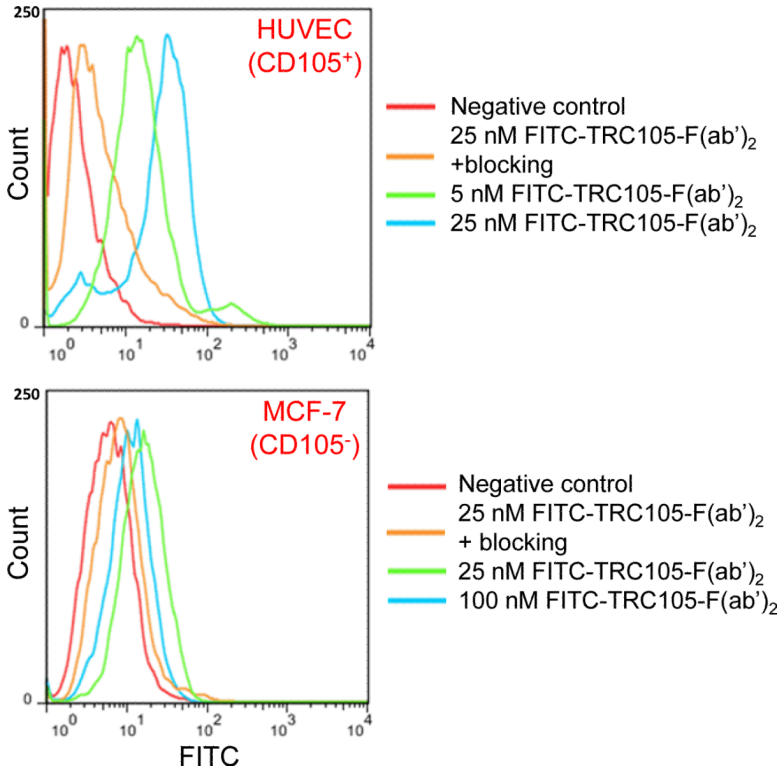

Figure 2.
Flow cytometry analyses in CD105-positive HUVEC and CD105-negative MCF-7 cells confirmed the specificity and affinity of TRC105-F(ab')$_2$ for CD105.

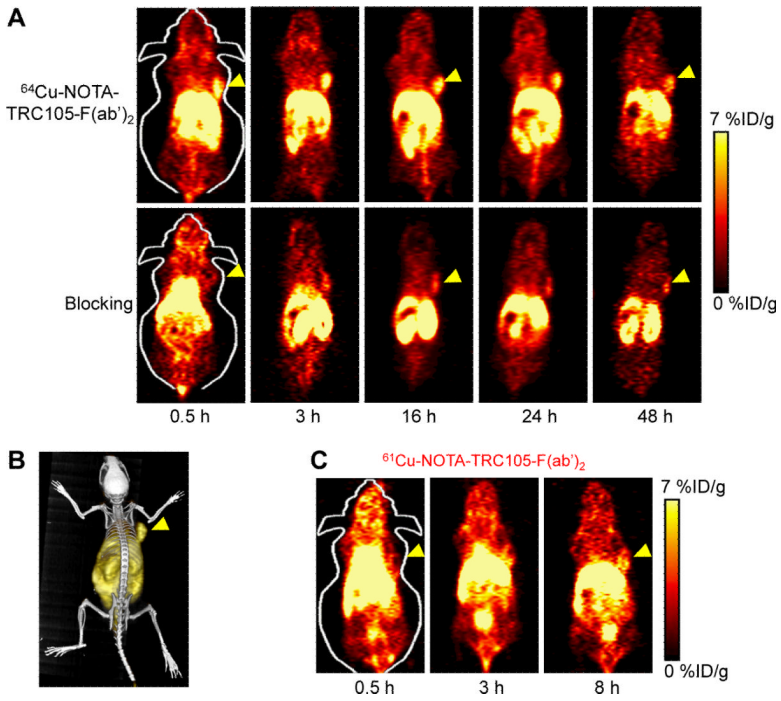

Figure 3.

Serial PET imaging of CD105 in 4T1 tumor-bearing BALB/c mice. (A) Serial coronal PET images at 0.5, 3, 16, 24, and 48 h post-injection of ^{64}Cu-NOTA-TRC105-F(ab')$_2$, or ^{64}Cu-NOTA-TRC105-F(ab')$_2$ after a pre-injected 1 mg dose of TRC105 (i.e. blocking). (B) A representative PET/CT image of 4T1 tumor-bearing mice at 3 h post-injection of ^{64}Cu-NOTA-TRC105-F(ab')$_2$. C. Serial coronal PET images at 0.5, 3, and 8 h post-injection of ^{61}Cu-NOTA-TRC105-F(ab')$_2$ in 4T1 tumor-bearing mice.

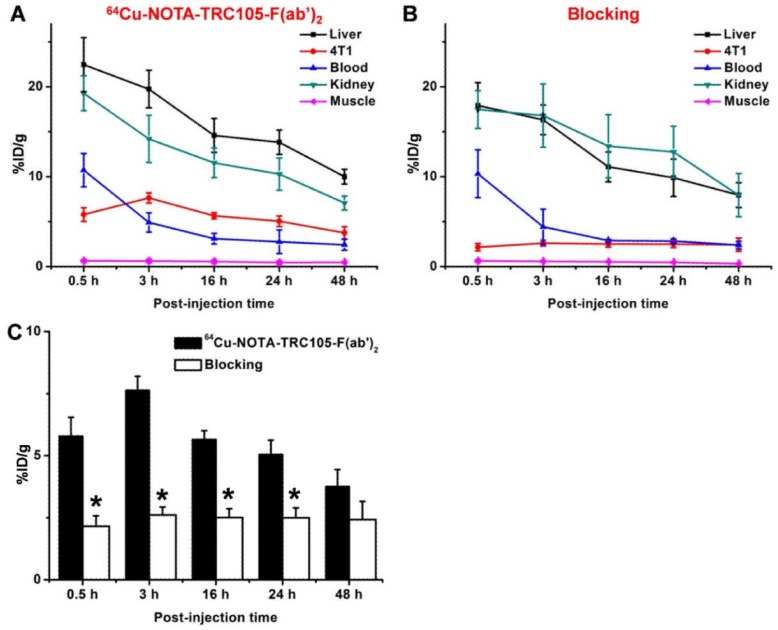

Figure 4.

Quantitative analysis of the PET data. (A) Time-activity curves of the liver, 4T1 tumor, blood, kidney, and muscle upon intravenous injection of ^{64}Cu-NOTA-TRC105-F(ab')$_2$. (B) Time-activity curves of the liver, 4T1 tumor, blood, kidney, and muscle upon intravenous injection of ^{64}Cu-NOTA-TRC105-F(ab')$_2$, after a blocking dose of TRC105. (C) Comparison of tracer uptake in the 4T1 tumors between the two groups. $n = 4$; *, $P < 0.05$.

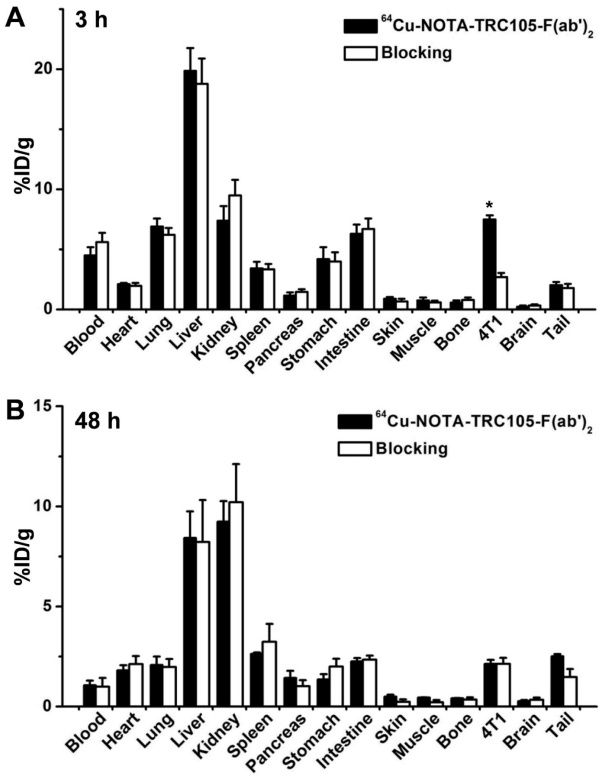

Figure 5.
Biodistribution of ^{64}Cu-NOTA-TRC105-F(ab')$_2$, or ^{64}Cu-NOTA-TRC105-F(ab')$_2$ after a blocking dose of TRC105, in 4T1 tumor-bearing mice at 3 h (A) or 48 h (B) post-injection. $n = 4$; *, $P < 0.05$.

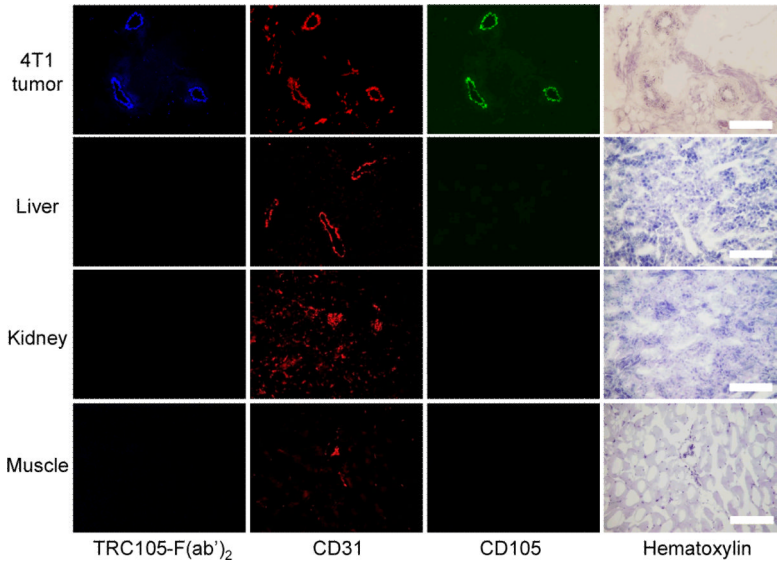

Figure 6.

Immunofluorescence CD105/CD31/AlexaFluor350-TRC105-F(ab')$_2$ triple staining of 4T1 tumor, liver, kidney, and muscle tissue sections. TRC105 and AlexaFluor488-labeled goat antihuman IgG were used for CD105 staining (green). Rat antimouse CD31 antibody and Cy3-labeled donkey antirat IgG were used for CD31 staining (red). AlexaFluor350-TRC105-F(ab')$_2$ was used (blue) to evaluate its overlay with CD105/CD31 staining. Hematoxylin staining was also conducted to reveal the location of cell nuclei. Magnification: 200 ×. Scale bar: 50 μm.